Artificial Organs
28(11):1026–1034, Blackwell Publishing, Inc.

Modeling Centrifugal Cell Washers Using Computational Fluid Dynamics

Beth E. Kellet, Binbing Han, David S. Dandy, and S. Ranil Wickramasinghe

Department of Chemical Engineering, Colorado State University, Fort Collins, CO, U.S.A.

Abstract: Reinfusion of shed blood during surgery could avoid the need for blood transfusions. Prior to reinfusion of the red blood cells, the shed blood must be washed in order to remove leukocytes, platelets, and other contaminants. Further, the hematocrit of the washed blood must be increased. The feasibility of using computational fluid dynamics (CFD) to guide the design of better centrifuges for processing shed blood is explored here. The velocity field within a centrifuge bowl and the rate of protein removal from the shed blood has been studied. The results obtained indicate that CFD could help screen preliminary centrifuge bowl designs, thus reducing the number of initial experimental tests required when developing new centrifuge bowls. Although the focus of this work is on washing shed blood, the methods developed here are applicable to the design of centrifuge bowls for other blood-processing applications. **Key Words:** Centrifugal cells washers—Computational fluid dynamics—Blood—Velocity field—Protein removal.

Centrifuges are widely used to process human blood. Whole blood is routinely fractionated by centrifugation into components such as plasma, red blood cells, platelets, and leukocytes. The name given to the centrifugation-based separation depends on the specific application. Therapeutic apheresis is used for the treatment of a variety of diseases and disorders characterized by the presence of abnormal proteins or blood cells in the circulation, which are believed to be involved in the propagation of that condition (1). When the blood component to be treated is the plasma, the apheresis technique is termed plasmapheresis. Plasmapheresis is used in the treatment of a number of diseases such as Waldenstrom's syndrome, glomerulonephritis, and myasthenia gravis. When the component of the blood to be treated is cellular, the process is termed cytapheresis. Examples of cytapheresis techniques include treatment of diseases such as leukemia (cytapheresis, used to remove leukocytes) and sickle cell anemia (erythrocytapheresis, used to remove red blood cells) (2). In all of these apheresis techniques, the fractionation of blood into its basic components is frequently achieved by centrifugation.

Today, blood-banking practice is moving away from the transfusion of whole blood (3). Donated blood is first separated into relatively pure fractions. Plastic bag systems are available, which enable the preparation by centrifugation of units of red blood cell concentrates, platelets, and plasma from whole blood in a closed system thus, avoiding the possibility of contamination. Further, donor apheresis techniques, such as donor plasmapheresis, are also used to collect only the desired components from the donor. Thus, centrifugation is frequently used in blood banks for blood processing.

Due to the risk of hemolytic reactions, immune responses, and the transmission of blood-borne pathogens, there is a great need to minimize the number of transfusions required during major surgery. Frequently, the patient's own blood (shed blood) is collected during surgery, processed, and reinfused thus, minimizing the requirements for transfusion of red blood cells (4–7). Because irrigation fluids are used during surgery, the shed blood has a very low hematocrit. Leukocytes and platelets are often activated in shed blood, thus it is undesirable to reinfuse them. Processing shed blood involves centrifugation to concentrate and purify the red blood cells present.

Received June 2003; revised October 2003.
Address correspondence and reprint requests to Dr. S. Ranil Wickramasinghe, Department of Chemical Engineering, Colorado State University, Fort Collins, CO 80523, U.S.A. E-mail: wickram@engr.colostate.edu

Designing optimized centrifuges for blood processing is a complicated process. Here, we consider the use of computational fluid dynamics (CFD) as a tool for designing centrifuges. We focus on centrifuges for processing shed blood. An optimized centrifuge is one that maximizes the recovery of highly purified concentrated red blood cells. Further, it is desirable that small volumes (about 100 mL) of shed blood be processed as quickly as possible for rapid reinfusion. The CFD analysis developed here may be used as a tool when designing centrifuges for other blood-processing applications.

Previous studies have investigated the use of CFD as a design tool for biomedical devices. For example, CFD models have been used in the development of new blood oxygenator designs by several researchers (8–10). These investigators found that CFD models could help guide new blood oxygenator designs.

Numerous studies have considered the design of blood pumps. Miyazoe et al. (11,12) and Tsukamoto et al. (13) investigated the use of CFD as a design tool for centrifugal blood pumps. They found that a three-dimensional CFD model was a useful design tool when combined with flow visualization results and hemolysis tests. Apel et al. (14) quantified shear-induced hemolysis in a microaxial blood pump using CFD. They found that CFD was a convenient design tool for the general assessment of shear-induced hemolysis. Burgreen et al. (15) present a detailed assessment of the value of CFD in the design of a rotary blood pump. The blood-contacting surfaces of the pump were designed based on their CFD analysis. They found that their CFD model eliminated the need to build a prototype after each geometric refinement, resulting in savings of time and money.

We have developed and applied an axisymmetric CFD model of the centrifuge bowl used in the COBE BRAT 2 (COBE Cardiovascular, Arvada, CO, U.S.A.). The CFD model is used to compute the liquid velocity and pressure fields in the bowl and the removal of plasma proteins from the shed blood as functions of the inlet fluid flow rate and centrifugation rate.

MATERIALS AND METHODS

The COBE BRAT 2 is an autologous transfusion system that is designed to provide washed red blood cells. The key component of the BRAT 2 is the centrifuge bowl known as a Baylor Bowl (16). Figure 1 is a photograph of the centrifuge bowl while Fig. 2 shows cross-sectional and plane views. Blood enters via a central inlet tube and flows to the bottom of the bowl. Next, the blood is forced radially along the bottom toward the outer wall of the bowl. As shown in Fig. 2, the blood flows around a fin that protrudes from the bottom of the inside spacer. The blood then flows upward between the inside spacer and the outer casing to the outlet located at the top of the centrifuge bowl. The outer casing of the bowl and the inside spacer are connected and rotate at approximately 4400 rpm. The densities of the cellular blood components are: 1090–1100 kg/m^3 for red blood cells; 1050–1085 kg/m^3 for leukocytes; and 1040–1060 kg/m^3 for platelets (17–19). Consequently, the red blood cells deposit on the outer wall of the centrifuge bowl while the leukocytes and platelets tend to deposit on top of the red blood cells. The plasma flows upward between the deposited cells and the inside spacer toward the exit located at the top of the bowl. Blood to be processed is loaded into the centrifuge bowl until the red blood cells are detected by a sensor located at the top of the bowl. Next, wash solution is added. The aim of the washing process is to remove plasma proteins and to ensure minimal contaminant of the deposited red blood cells by trapped leukocytes and platelets. The bottom edge of the inside spacer contains the fin (see Fig. 2). The fin ensures that the wash solution is forced through the deposited red blood cells, thus enhancing the removal of plasma proteins and trapped leukocytes and platelets. Finally, the red blood cells are concentrated. The processed red blood cells are discharged by reversing the direction of liquid flow. A CFD model of the centrifuge bowl was developed to determine the liquid flow field within the bowl and the rate of removal of plasma proteins.

FIG. 1. Centrifuge bowl modeled in this study.

CFD MODEL

The continuity and Navier–Stokes equations for an incompressible liquid are used in this study,

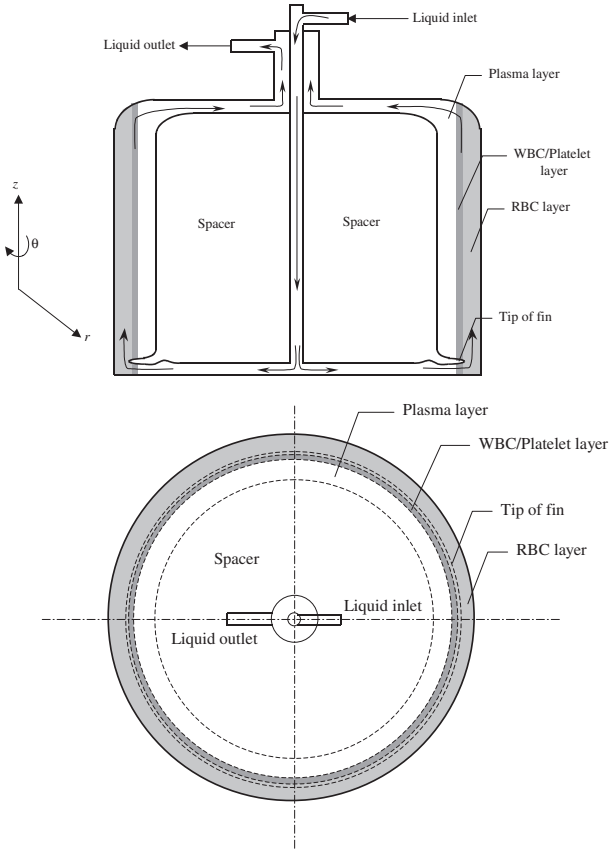

FIG. 2. Cross-sectional and plane view of centrifuge bowl.

$$\nabla \cdot V = 0 \tag{1}$$

$$\rho \frac{DV}{Dt} = -\nabla P + \rho g + \mu \nabla^2 V \tag{2}$$

where V is the velocity, ρ is the liquid density, P is the pressure, t is the time, g is the gravitational constant, and μ is the liquid viscosity. Cylindrical coordinates (r, θ, z) are used. Although there is an appreciable velocity component in the θ direction due to the axisymmetric geometry of the centrifuge bowl (see Fig. 2), velocity and pressure are independent of this coordinate. At all liquid solid interfaces, the Navier no-slip boundary condition is assumed. In addition, a flat inlet velocity profile is used as a boundary condition because numerical experiments showed that the velocity profile was fully developed at the fin tip, regardless of the specific inlet condition.

A model of the bowl was built using ProEngineer (Parametric Technology Corporation, MA, U.S.A.). The model was converted to an initial graphics exchange specification (IGES) format and then imported into a preprocessor called Gambit (Fluent, Lebanon, NH, U.S.A.). Within Gambit, the flow domain was discretized into cells. The resulting meshed geometry contained over 43 000 cells. It was found that using a smaller number of cells (a coarser mesh) led to a grid-dependent solution. Figure 3 shows the meshed flow domain. The meshed flow domain was then imported into Fluent (Fluent, Lebanon, NH, U.S.A.).

Two simulations were carried out. In the first simulation, water flowed through a centrifuge bowl spinning at 4400 rpm. This simulation gives the velocity field within the centrifuge bowl. In the second simulation, it was assumed that the bowl was filled with blood. The washing process, using saline, was then simulated. This simulation gives the rate of protein removal. For both simulations, it was assumed that the inlet fluid velocity profile was flat (i.e., plug flow). A liquid flow rate of 200 mL/min was used as this is typical of the values encountered in practice. The no-slip boundary condition for all tangential velocities was applied at all solid liquid interfaces. The density and viscosity of the liquid (water and saline) was assumed to be that of water at 25°C: 998 kg/m^3 and 0.001 Pa s, respectively. Because the first simulation gives the steady state velocity field in the bowl, it is time-independent. The second simulation gives the change of protein concentration within the bowl as a function of time for a 5-minute washing cycle.

In addition, for the second simulation, it was assumed that the bowl was filled with liquid. The inlet hematocrit was taken as 10%, a typical value in practice. The plasma proteins were modeled using albumin. The diffusivity of albumin was taken as 1×10^{-11} m^2/s, which was calculated from the Einstein–Stokes equation (20) at the experimental

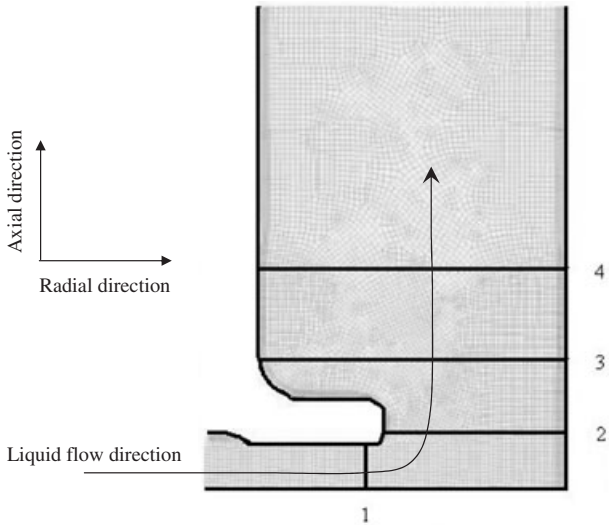

FIG. 3. Part of the meshed section of the bowl and locations of radial and axial velocity profiles.

conditions. The inlet protein concentration was 174 g/L in the plasma. Finally, it was necessary to model-flow through the region of deposited red blood cells. This was achieved using the porous flow model, based on Darcy's law, built into the Fluent software. Because the commercial Fluent software used here cannot account for the deformability of red blood cells, the deposited red blood cells were assumed to consist of rigid particles. Clinical data indicate that the pressure drop for flow through the bowl is between 6.89 and 13.8 kPa (1–2 psi). If a porosity of 20% is assumed for the deposited red blood cells, a pressure drop of 10.3 kPa (1.5 psi) is obtained. Further, by defining a porosity for the layer for deposited cells, the thickness of the deposited layer is specified because the inlet hematocrit of the blood was 10%. Thus, the deposited layer of red blood cells was modelled as a region of 20% porosity such that the resistance to liquid flow was the same as observed in practice. In this study, the presence and the removal of leukocytes and platelets were ignored.

RESULTS

CFD simulation results were obtained for the velocity field within the bowl and the rate of protein removal.

Simulation 1 velocity field within the bowl

From Fig. 3, it can be seen that large changes in liquid velocity occur near the fin as the direction of liquid flow changes from radial to axial. Consequently, velocity and pressure profiles were obtained at various locations near the tip of the fin as well as

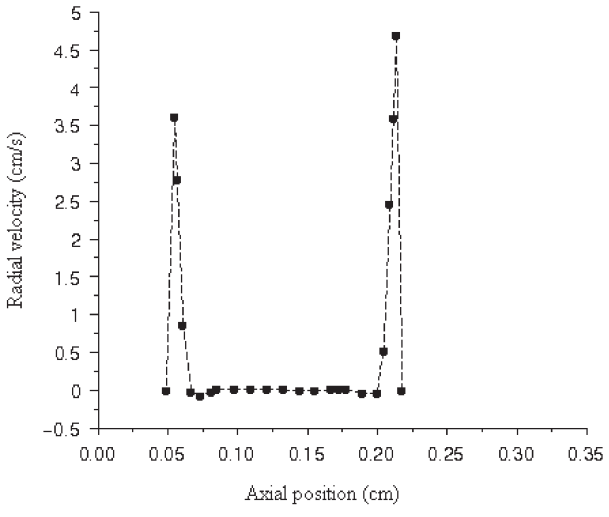

FIG. 4. Velocity profile at location 1 (see Fig. 3) in simulation 1.

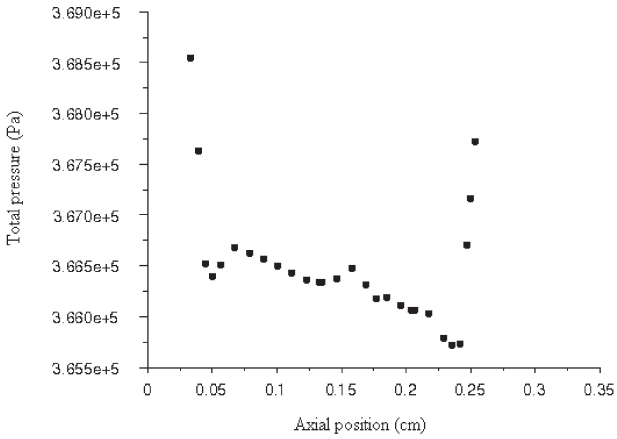

FIG. 5. Pressure profile at location 1 (see Fig. 3) in simulation 1.

at various axial locations shown in Fig. 3. At location 1, the fluid is flowing along the bottom of the bowl toward the outer edge of the bowl. The corresponding velocity and total pressure profiles are given in Figs. 4 and 5, respectively. Figure 4 indicates the existence of two flow channels, one near each solid surface. At the surface of the flow channel, the liquid velocity is zero because the Navier no-slip boundary condition was assumed. Figure 5 shows that a large pressure gradient exists very close to the upper and lower surfaces of the flow channel. This is due to the large velocity gradient that exists in the two flow channels (see Fig. 4). Because the inlet fluid velocity profile was assumed to be flat, the observed radial velocity field develops over a very short distance. Importantly, the velocity near the center of the flow channel is close to zero.

Axial velocity and total pressure profiles at various locations marked 2–4 in Fig. 3 are given in Figs. 6 and 7, respectively. Near the fin (location 2), a single axial flow channel exists next to the outer surface of the fin. The velocity in this channel starts to decrease as one moves along the axis of the bowl toward the top of the bowl. However, two additional flow channels develop as one moves toward the top of the bowl (locations 3 and 4): one near the inner surface of the bowl and one in between the other two flow channels. Regions of negative (downward) velocity also exist. The location of the first negative velocity is near the tip of the fin at a radial distance a little greater than the outermost flow channel. The magnitude of the negative velocity in this flow channel rapidly decreases as one moves toward the top of the bowl. Two other regions of negative velocity occur on either side of the centrally located flow channel at locations 3 and 4 (Fig. 3). The existence of these regions of negative velocity indicates that there is

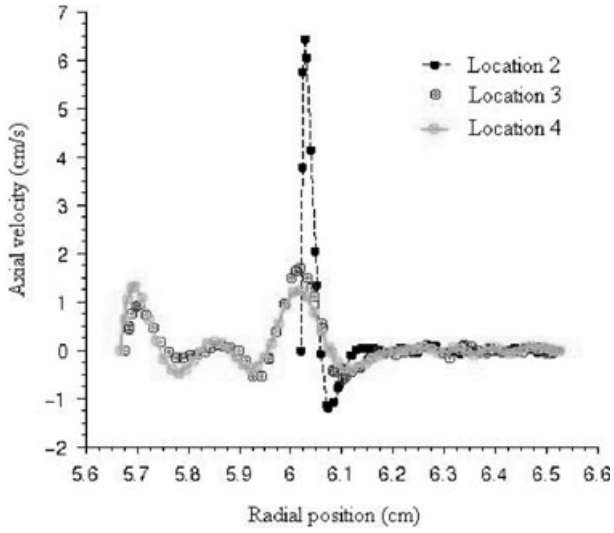

FIG. 6. Velocity profile at locations 2, 3, and 4 (see Fig. 3) in simulation 1. The inner surface of the casing and surface of the inner spacer define the region occupied by the blood. The inner surface of the casing and the surface of the inner spacer have a radial position of 6.55 and 5.675 cm, respectively, while the outer surface of the fin has a radial position of 6.025 cm.

recirculation of liquid within the bowl. Figure 6 also indicates that most of the fluid between the outer surface of the bowl and the outermost negative flow channel is stagnant. At the outer and inner surfaces of the bowl, the liquid velocity is zero as enforced by the Navier no-slip boundary condition.

The corresponding total pressure profiles given in Fig. 7 indicate that the total pressure varies approximately linearly with radial position. By comparing

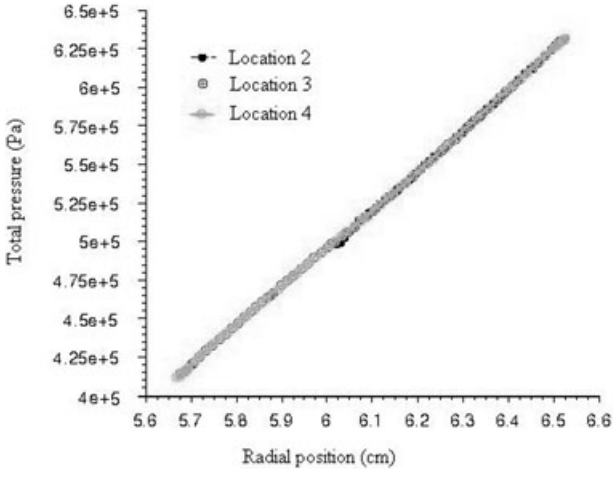

FIG. 7. Pressure profile at locations 2, 3, and 4 (see Fig. 3) in simulation 1. The inner surface of the casing and surface of the inner spacer define the region occupied by the blood. The inner surface of the casing and the surface of the inner spacer have a radial position of 6.55 and 5.675 cm, respectively, while the outer surface of the fin has a radial position of 6.025 cm.

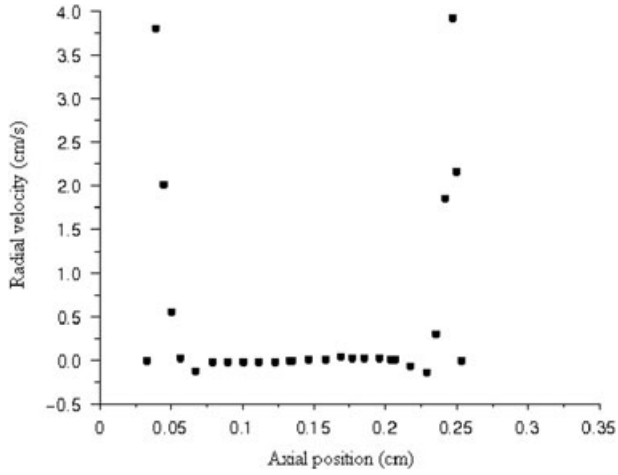

FIG. 8. Velocity profile at location 1 (see Fig. 3) in simulation 2.

Figs. 5 and 7, it can be seen that the variation of the total pressure at each axial location (locations 2, 3, and 4 in Fig. 3) is much greater than the variation of total pressure across the radial location (location 1 in Fig. 3). Consequently, slight variations in the total pressure due to the axial liquid velocity are not observed. In Fig. 5 on the other hand, the variation in total pressure is less than 3000 Pa, consequently variations due to radial liquid flow are clearly visible.

Simulation 2 protein removal

The second simulation assumes that the bowl is fully loaded and that cell washing has begun. Consequently, there is a layer of deposited red blood cells at the outer surface of the bowl. Velocity and pressure profiles were determined at the same locations as the first simulation (see Fig. 3). The radial velocity and total pressure variations at location 1 are given in Figs. 8 and 9, respectively. By comparing Figs. 4

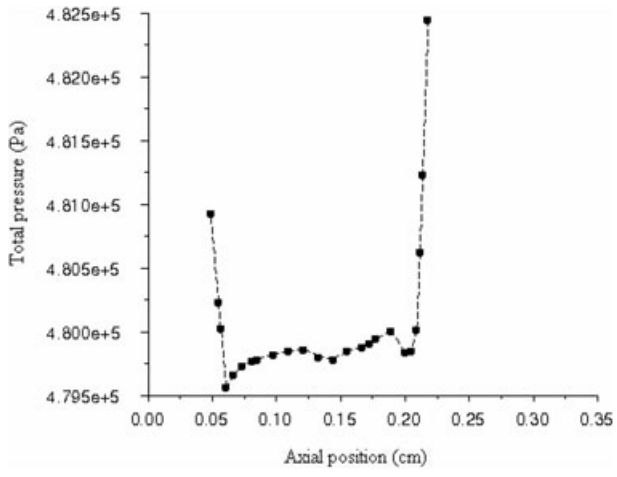

FIG. 9. Pressure profile at location 1 (see Fig. 3) in simulation 2.

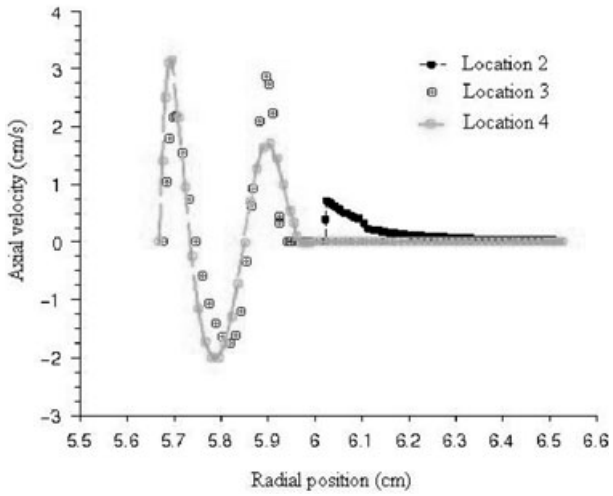

FIG. 10. Velocity profile at locations 2, 3, and 4 (see Fig. 3) in simulation 2. The inner surface of the casing and surface of the inner spacer define the region occupied by the blood. The inner surface of the casing and the surface of the inner spacer have a radial position of 6.55 and 5.675 cm, respectively, while the outer surface of the fin has a radial position of 6.025 cm.

and 8, it can be seen that qualitatively, the figures are similar. However, the presence of a layer of deposited red blood cells in the centrifuge bowl results in the radial velocity in the two flow channels being approximately the same, unlike in Fig. 4. By comparing Figs. 5 and 9, it can be seen that the presence of deposited red blood cells changes the pressure profile. The total pressure is higher at all points.

Axial velocity and total pressure profiles at various locations marked 2–4 in Fig. 3 are given in Figs. 10 and 11, respectively. The axial velocity fields given in Fig. 10 are quite different to those in Fig. 6. The flow channel near the outer edge of the fin is now within the deposited red blood cells. Consequently, it disappears very quickly as one move toward the top of the bowl. Two other flow channels develop: one near the inner wall of the bowl and one at the cell–liquid interface. In between the two flow channels, there is a region of negative velocity indicating recirculation of the fluid. By comparing Figs. 6 and 10, it is seen that the degree of recirculation is greater in Fig. 10. The liquid appears to be stagnant within the region of deposited red blood cells.

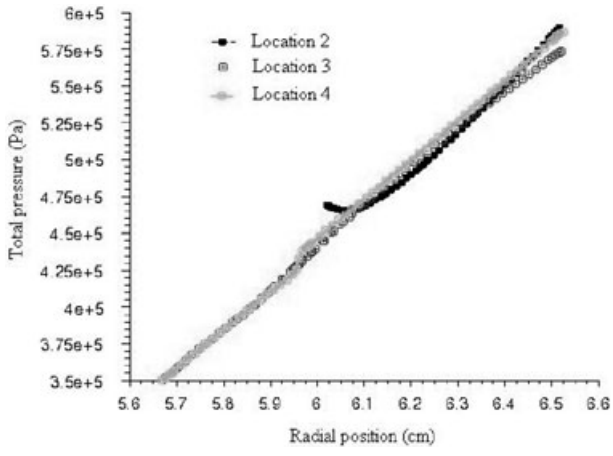

FIG. 11. Pressure profile at locations 2, 3, and 4 (see Fig. 3) in simulation 2. The inner surface of the casing and surface of the inner spacer define the region occupied by the blood. The inner surface of the casing and the surface of the inner spacer have a radial position of 6.55 and 5.675 cm, respectively, while the outer surface of the fin has a radial position of 6.025 cm.

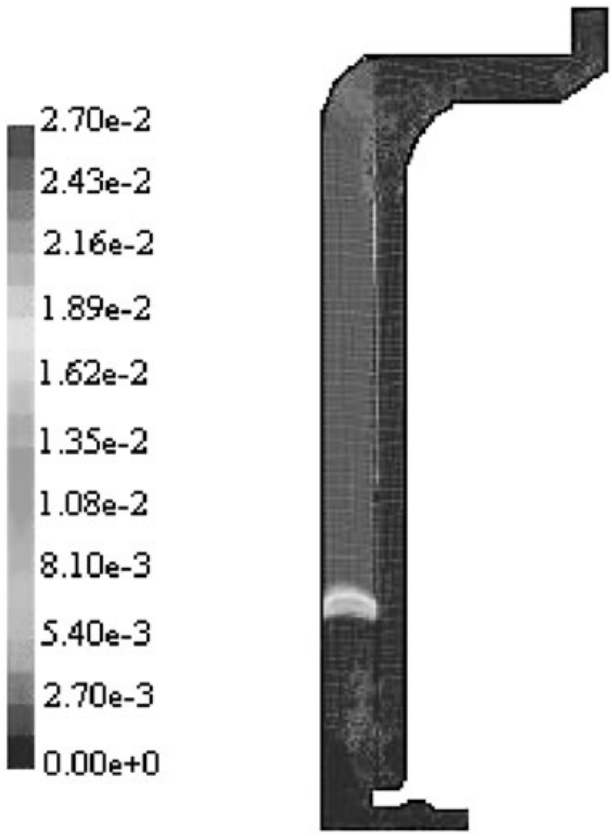

FIG. 12. Mass fraction of albumin in bowl after 5-min washing.

By comparing Figs. 7 and 11, it can be seen that the corresponding pressure profiles are similar. At location 2, a flow through the region of deposited red blood cells causes a deviation in the approximately linear pressure variation with radial position.

The variation of albumin concentration after 5 min is given in Fig. 12. As can be seen, the albumin present in the plasma has been completely removed. However, the removal of albumin in the layer of deposited red blood cells is incomplete. The CFD software treats the region of deposited red blood cells as a region of increased resistance to liquid flow.

However, the software does not account for the fact that 20% porosity implies that 80% by volume of the region of deposited red blood cells is not available for plasma, and therefore albumin. Rather, the software assumes that the entire volume may be occupied by the plasma; however, the resistance to flow is much higher, as specified by a porosity of 20%. Therefore, the current CFD model describes the removal of albumin qualitatively. Nevertheless, the model may be used empirically to obtain a semiquantitative prediction of the level of albumin removal as described in the next section.

DISCUSSION

During centrifugation, the contents of the bowl migrate to the outer wall. As liquid enters from the bottom of the bowl, it has to pass around the fin (see Fig. 2) before it can flow upward, parallel to the axis of rotation, and exit the bowl. In both simulations, a liquid flow rate of 200 mL/min was assumed. Figures 4 and 8 indicate the existence of two flow channels as the liquid flows along the bottom of the bowl. The existence of the upper flow channel next to the upper surface of the bowl (axial position of 0.05 cm, Fig. 4) is easy to explain. When the fluid reaches the fin, it starts to move upward, parallel to the axis of rotation. Thus, this flow channel represents the path of least resistance for liquid flow.

The flow channel at the lower surface of the bowl (axial position of 0.21 cm, Fig. 4) is more difficult to explain. It results from the diffusion of axial momentum. At the tip of the fin, as fluid moves upward along the axis of rotation, the fluid below it will be at a slightly higher pressure. This causes the fluid a little below to also move upward. This repeats itself all the way to the bottom surface of the centrifuge. However, because fluid is entering from the left (see Fig. 3), this leads to the creation of a second flow channel at the bottom surface of the bowl. Figures 4 and 8 indicate that, aside from these two flow channels, there is little fluid motion. As a consequence of the centrifugal force on the fluid at the outer surface of the bowl, fluid that is closer to the axis (which experiences a lower centrifugal force) is prevented from displacing it. Thus, there is a net resistance of fluid flow along the bottom channel, resulting in the fluid flow being restricted to two flow channels.

By comparing Figs. 4 and 8, it can be seen that the actual values of liquid velocities in the two flow channels are different in the two simulations at the same volumetric liquid flow rate. These differences are caused by the fact that in the second simulation, the liquid in both flow channels must flow through a region of deposited red blood cells. The corresponding pressure profiles, Figs. 5 and 9 are similar but also indicate the effect of the deposited red blood cells. Figure 9 shows that the presence of red blood cells leads to a higher overall pressure.

Figures 6 and 10 give the axial velocity as a function of radial position for the two simulations at positions 2–4 (see Fig. 3). Both figures show a rather large initial axial velocity at a radial position corresponding to the outer surface of the tip. This represents the liquid as it flows around the fin. However, the axial velocity in this flow channel decreases with increasing axial position (from the bottom of the bowl). Due to the centrifugal force, the resistance to axial flow is least at the surface of the inside spacer (lowest centrifugal force). Thus, as axial velocity in the initial axial flow channel decreases, new flow channels develop closer to the surface of the inside spacer. The changes in axial velocity in the various flow channels are more dramatic in Fig. 10. The reason is that the initial flow channel in this case lies completely inside the layer of deposited red blood cells, thus the resistance to axial flow is significantly higher compared to the first simulation. Figures 6 and 10 indicate regions of negative velocity indicating the existence of recirculation. This is significant because recirculation will compromise the efficiency of protein removal, which is an important design consideration. The corresponding pressure profiles indicate a rapid increase in pressure at the outer wall of the bowl. Further, variations in pressure due to axial fluid motion are masked by the strong dependence of the pressure on radial position due to the centrifugal force.

Figures 7 and 11 show the pressure profile for the two simulations at locations 2, 3, and 4 as a function of radial position (see Fig. 3). Both figures show that, as distance from the axis of rotation increases, the total pressure increases approximately linearly. The total pressure is the sum of static pressure and dynamic pressure due to the axial and angular velocity of the fluid. For a given axial location (2, 3, or 4), the static pressure is constant. Because the largest axial velocity is less than 7 cm/s (see Fig. 6) while the angular velocity is about 4400 rpm, the total pressure will be dominated by the dynamic pressure due to the angular velocity of the fluid. Consequently the pressure gradient is given by,

$$\frac{dP}{dr} = \rho\omega^2 r \tag{3}$$

where ω is the angular velocity and r is the distance from axis of rotation. Integrating the above equation,

$$P = \frac{1}{2}\rho\omega^2 r^2 + c_1 \tag{4}$$

TABLE 1. *Clinical data for albumin removal using the BRAT 2 (Data provided by COBE Cardiovascular, Arvada, CO, U.S.A.)*

Run	Inlet albumin concentration (g/L)	Outlet albumin concentration (g/L)	Removal percent (%)
1	20.7	1.02	95
2	20.7	0.895	96
3	20.7	0.872	96
4	20.7	0.851	96

where c_1 is an constant of integration.

The total pressure varies with the square of the radial position. However, because the radial distances given in Figs. 7 and 11 are small, 5.7–6.6 cm, the variation of total pressure with radial position appears linear.

The removal of albumin is shown qualitatively in Fig. 12. As can be seen, a saline front develops in the deposited red blood cells, which slowly moves upward toward the exit of the centrifuge. Figure 12 shows the position of the front after 5 min. Table 1 gives clinical data for the percentage of residual albumin after cell washing for the conditions used in this simulation (inlet hematocrit 10%, flow rates for fill and wash cycles 200 mL/min, wash time 5 min).

The CFD model may be used to predict semiquantitatively the percentage removal of albumin by dividing the centrifuge bowl into two zones. The zone that contains the plasma is assumed to have an albumin concentration equivalent to the initial measured supernatant albumin concentration. The albumin concentration in the zone containing deposited red blood cells is determined by first calculating the total mass of albumin present, that is, supernatant albumin concentration multiplied by the porosity of the zone (20% in this study). The calculated mass of albumin is then divided by the total volume of the zone (including red blood cells). Thus, the centrifuge bowl is divided into two zones with different initial albumin concentrations. Using this method, the predicted albumin removal is 90%, which is a little less than obtained in clinical studies (see Table 1).

The CFD method that is used to predict the residual albumin in the washed blood is based on a number of assumptions. Firstly, to account for the fact that the volume occupied by red blood cells is not available for supernatant albumin, the albumin concentration in the zone containing deposited red blood cells is artificially adjusted. Further, the porous flow model employed by the CFD program does not rigorously account for the tortuous liquid flow path within the zone of deposited red blood cells. Nevertheless, the current CFD model may be used to indicate the effect of varying processing parameters such as the wash time and liquid flow rate on albumin removal.

The results of the two simulations presented here indicate that CFD may be a useful tool when designing more efficient centrifuges for blood processing. For example, the velocity fields indicate the presence of recirculation within the bowl, which will compromise performance. Simulations of new bowl designs could be run to determine which ones indicate reduced recirculation. By only testing bowl designs that appear promising, CFD simulations could be used to screen new bowl designs reducing the number of initial experimental tests required. Similarly, more realistic CFD models for the zone of deposited red blood cells could be developed, which in turn could provide initial estimates of protein removal. However, prediction of leukocyte and platelet removal will be more difficult as this involves the removal of interacting particles.

The results presented here focus on the use of CFD for washing shed blood. However, centrifuges are used throughout the blood banking industry for many blood-processing applications. The CFD methods described here may be used to determine the velocity field in centrifuge bowls for other blood-processing applications. Consequently, CFD could be a useful tool in designing centrifuges for other blood-processing applications.

Although semiquantitative agreement is obtained between numerical and experimental results for albumin removal, the predicted velocity and pressure profiles within the centrifugal cell washer have not been validated directly by experiment. Because albumin removal is dependent upon the velocity profile, which in turn depends on the pressure distribution within the centrifuge, the numerically determined velocity and pressure profiles appear accurate. However, before using CFD to design centrifuges, this should be verified.

CONCLUSION

A CFD model of the Baylor bowl used in the COBE Cardiovascular, BRAT 2 has been developed. Two simulations have been run, one representing the centrifuge bowl filled with water, and the second representing the bowl filled with blood. The first simulation was focused on determining the velocity and pressure fields within the bowl, while the second examined the predicted rate of protein removal. Both simulations indicate that zones of liquid recirculation exist within the bowl. However, the degree

of recirculation is greater when the centrifuge bowl is filled with blood. The model provides semiquantitative predictions of protein removal during cell washing. The result obtained here indicates that development of CFD models could be a valuable tool when designing more efficient centrifuges.

Acknowledgments: Financial support was provided by COBE Cardiovascular, Arvada, Colorado, and the Colorado Institute for Research in Biotechnology. The authors would like to acknowledge Dr. Steve Hunley for his many helpful suggestions.

REFERENCES

1. Zydney AL. Therapeutic apheresis and blood fractionation. In: Bronzino JD, ed. *The Biomedical Engineering Handbook*. Boca Raton: CRC Press, 1995;1936–51.
2. Sawada K, Malchesky PS, Nosé Y. Available removal systems: state of the art. In: Nydegger UE, ed. *Therapeutic Hemapheresis in the 1990s*. New York: Karger, 1990;51–113. *(Current studies in hematology and blood transfusion*, Vol. 57).
3. Wickramasinghe SR. Washing cryopreserved blood products using hollow fibres. *Trans Icheme* 1999;77:287–92.
4. Kongsgaard UE, Hovig T, Brosstad F, Geiran O. Platelets in shed mediastinal blood used for postoperative autotransfusion. *Acta Anaesthesiol Scand* 1993;37:265–8.
5. Schmidt H, Kongsgaard UE, Kofstad J, Geiran O, Refsum HE. Autotransfusion after open heart surgery: the oxygen delivery capacity of shed mediastinal blood is maintained. *Acta Anaesthesiol Scand* 1995;39:754–8.
6. Vertrees RA, Conti VR, Lick SD, Zwischenberger JB, McDaniel LB, Shulman G. Adverse effects of postoperative infusion of shed mediastinal blood. *Ann Thorac Surg* 1996; 62:717–23.
7. Schönberger JPAM, Bredée J, Speekenbrink RG, Everts PAM, Wildevuur CRH. Autotransfusion of shed blood contributes additionally to blood saving in patients receiving aprotinin (2 millino KIU). *Eur J Cardiothorac Surg* 1993;7: 474–7.
8. Gartner MJ, Wilhelm CR, Gage KL, Fabrizio MC, Wagner WR. Modeling flow effects on thrombotic deposition in a membrane oxygenator. *Artif Organs* 2000;24:29–36.
9. Goodin MS, Thor EJ, Haworth WS. Use of computational fluid dynamics in the design of the avecor affinity oxygenator. *Perfusion* 1994;9:217–22.
10. Bludszuweit C. Evaluation and optimization of artificial organs by computational fluid dynamics. *Proceedings of the 1997 ASME Fluids Engineering Division Summer Meeting.* Vancouver, British Columbia, Canada, June 22–26, 1997.
11. Miyazoe Y, Sawairi T, Ito K, et al. Computational fluid dynamic analyses to establish design process of centrifugal blood pumps. *Artif Organs* 1998;22:381–5.
12. Miyazoe Y, Sawairi T, Ito K, et al. Computational fluid dynamics analysis to establish the design process of a centrifugal blood pump: second report. *Artif Organs* 1999;23:762–8.
13. Tsukamoto Y, Ito K, Sawairi T, et al. Computational fluid dynamics analysis of a centrifugal blood pump with washout holes. *Artif Organs* 2000;24:648–52.
14. Apel J, Paul R, Klaus S, Siess T, Reul H. Assessment of hemolysis related quantities in a microaxial blood pump by computational fluid dynamics. *Artif Organs* 2001;25:341–7.
15. Burgreen GW, Antaki JF, Wu ZJ, Holmes AJ. Computational fluid dynamics as a development tool for rotary blood pumps. *Artif Organs* 2001;25:336–40.
16. Carson GA. Method and apparatus for autologous blood salvage. US Patent 5 976 388, 1999.
17. Campbell N. *Biology*. Menlo Park: Benjamin/Cummings Publishing Co, 1996.
18. Bronzino J. *Introduction to Biomedical Engineering*. San Diego: Academic Press, 2000.
19. Zucker-Franklin D. Atlas of blood cells—function and pathology. Milano: EdiEremes, Italy, 1981.
20. Freitas RA Jr. *Nanomedicine, Vol. 1: Basic Capabilities.* Austin: Landes Bioscience, 1999.